ELSEVIER

Journal of Fluorine Chemistry 113 (2002) 185–194

JOURNAL OF FLUORINE CHEMISTRY

www.elsevier.com/locate/jfluchem

^{19}F NMR investigation of the $Pb_{1-x}Mg_xF_2$ solid solution

Malika El Omari[a], Mohamed El Omari[a], Jean-Maurice Réau[b], Jean Sénégas[b,*]

[a]*Département de Chimie, Faculté des Sciences, B.P. 4010, Béni M'hamed, Meknès, Morocco*

[b]*Institut de Chimie de la Matiere Condensee de Bordeaux (ICMCB), 87 Av. Dr. A. Schweitzer, 33608 Pessac Cedex, France*

Received 29 June 2001; accepted 27 September 2001

Abstract

An ^{19}F NMR investigation of the $Pb_{1-x}Mg_xF_2$ solid solution is undertaken as a function of temperature. Several F^- ion sublattices are identified, they become progressively mobile on the NMR time scale at increasing temperature. Clusters are proposed from the composition dependence of the anionic distribution determined by deconvolution of the low temperature ^{19}F NMR spectra. Temperature dependence of the jump frequency shows the existence of several F^- ion motions corresponding to exchange motions inside and between fluoride sublattices.

Keywords: Fluorides; F^- ion conductivity; ^{19}F NMR diffusion; Clustering

1. Introduction

The transport properties of F^- ion conductor fluorides are closely correlated to their short range structure. The anion-excess $M_{1-x}{}^{2+}M'_x{}^{2+\alpha}F_{2+\alpha x}$ solid solutions with fluorite-type structure, which can involve various host and substitutional cations and offer large existence ranges, are a typical case and clustering actually has an essential influence on their transport properties. A clustering process model inside these solid solutions has been proposed relating, in a continuous way, the composition dependence of electrical properties and the progressive extension of clustering when x increases [1–3]. The fundamental features of the defect structure in long range disordered $M_{1-x}{}^{2+}M'_x{}^{2+\alpha}F_{2+\alpha x}$ solid solutions are well established. The fluorite-type structure MF_2 can be described as a cubic packing of F^- ions, where the M^{2+} cations occupy alternatively half of the cubic sites. Within solid solutions, two steps can be considered when x increases: for very low x values ($x \leq 0.01$), the charge compensating excess anions are located in interstitial sites, constituting point defect pairs of *nn* or *nnn* type [4,5] and, for higher x values, more extended defects, i.e. clusters, are formed. Such clusters, labeled n_1:n_2:n_3:n_4, are based on the association of n_1 vacancies in the (F_n) normal positions (1/4, 1/4, 1/4) of the fluorite-type network, n_2F' (1/2, u, u: $0.35 \leq u \leq 0.40$), n_3F'' (v_1, v_1, v_1: $v_1 \approx 0.41$) and n_4F''' (v_2, v_2, v_2: $0.28 \leq v_2 \leq 0.33$) interstitial fluorides with n substitutional cations [2,6,7]. Clustering induces significant transfer of fluoride ions from normal positions into interstitial sites with formation of vacancies in the normal F_n sublattice. It results in an enhancement of the F^- ion conductivity with increasing x in the ($x \leq x_s$) range, where x_s is the substitution content for which the number of $(F_i)_m$ interstitial ions responsible for long range motions is maximum in each solid solution [2,3].

Application of the clustering process model to fluorite-type anion-excess solid solutions has allowed various clustering mechanisms to be proposed on the basis of neutron diffraction results associated with those obtained by impedance spectroscopy and ^{19}F NMR investigations [1–3]: larger and larger extension of column clusters in, for instance, $Pb_{1-x}M'_x{}^{2+\alpha}F_{2+\alpha x}$ ($M' = Al, Zr, In, Bi$) [2–8], progressive transformation of 4:4:3:0 clusters into 8:12:1:0 cubooctahedral clusters in, for example, $Ba_{1-x}Bi_xF_{2+x}$ [9] and $Ca_{1-x}M'_xF_{2+x}$ ($M' = Y, Er, Lu$) [10], progressive transformation of 4:0:3:3 clusters into condensed 2:0:6:0 clusters in, for example, $M_{1-x}M''_xF_{2+2x}$ ($M = Ca, Sr; M'' = Th, U$) [11]. All these solid solutions, characterized by the presence of trivalent or tetravalent guest cations, involve a high number of F^- ions located in interstitial sites; such a state appears, a priori, less probable when the substitutional cation is isovalent as there is no charge compensating excess anion. However, the substitution of SnF_2 and MgF_2 to PbF_2 inside fluorite-type $Pb_{1-x}Sn_xF_2$ [12] and $Pb_{1-x}Mg_xF_2$ [13,14] solid solutions results in an enhancement of F^- ion conductivity. What can be then the short range order? We are interested here in the lead–magnesium solid solution where local

* Corresponding author. Tel.: +33-55-684-6260; fax: +33-55-684-2761.
E-mail address: senegas@icmcb.u-bordeaux.fr (J. Sénégas).

0022-1139/02/$ – see front matter
PII: S0022-1139(01)00540-1

distortions are expected, resulting from the large size difference between both cations. Consequently, an investigation of $Pb_{1-x}Mg_xF_2$ by ^{19}F NMR has been undertaken as a function of temperature in the range 125–435 K. The goal of this study was to obtain information on the eventual existence of several fluoride sublattices at low temperature and to propose short range order in agreement with the composition dependence of electrical properties.

The ^{19}F NMR experiments have been made in static conditions; this technique has been applied successful to the $Pb_{1-x}Al_xF_{2+x}$ solid solution, where a cluster model has been proposed from deconvolution of the rigid lattice spectra at low temperature [13,14] and confirmed by neutron diffraction study [8]. On the other hand, it has recently been shown that magic angle spinning (MAS) ^{19}F NMR provides a novel and interesting method for probing mechanisms for motions in ionic conductors [15–17]: a mechanism of exchange between two inequivalent sublattices has been in that way evidenced in α-PbF_2 [17]; this method is very sensitive, but difficult to apply to ionic conductors with high conductivity, where the exchange mechanisms can arise at very low temperature.

2. Experimental

The different $Pb_{1-x}Mg_xF_2$ ($0 \leq x \leq 0.11$ at $T \approx 720$ K) compositions studied correspond to $x = 0.03$, 0.06 and 0.09. They were synthesized by solid state reaction from mixtures of binary fluorides homogenized in a glove box. The reactions were carried out in gold tubes under dry argon over 15 h at 1023 K. All treatments were followed by quenching to room temperature. The powder X-ray diffraction patterns are characteristic of a fluorite-type unit-cell, with a parameter a_c which does not vary notably with x, result in agreement with the previous data [18].

The $Pb_{1-x}Mg_xF_2$ samples used for the ^{19}F NMR investigation were introduced into quartz cylindrical tubes in a glove box. The tubes were then closed carefully in order to avoid any contamination of the samples during their experimental study. The ^{19}F NMR experiments were performed on a Bruker MSL-200 spectrometer ($B_0 = 4.7$ T) equipped with a standard variable temperature unit in the range 125–435 K. Each sample investigated was first cooled at 100 K and kept at that temperature for 2 h, then, maintained at each measurement temperature for 1 h in order to acquire a good thermal stability. Storage of a large number of measurements acquired over a 1 h period results in a high resolution signal. The ONEPULSE acquisition program [19] has been used in the operating conditions gathered in Table 1. This program has been selected, because the fluoride anions in $Pb_{1-x}Mg_xF_2$ have different diffusion coefficients. The data so obtained were processed by Fourier transformation, using the WINNMR 1D program [20].

Each ^{19}F NMR spectrum was simulated by use of the WINFIT program [21], which allows variation of peak position, peak height, linewidth, ratio of Gaussian to Lorentzian functions and relative percentage of their areas. When a single Gaussian does not fit exactly with the registered spectrum, an appropriate mixing of Gaussian and Lorentzian functions is used for simulation. This was the case in particular for the spectra relative to the motional narrowing temperature range.

Table 1
Experimental conditions of the ^{19}F NMR investigation of the $Pb_{1-x}Mg_xF_2$ solid solution

Spectrometer frequency (MHz)	188.283
Pulse width (μs)	0.7
Dead time delay (μs)	6
Recycle delay time (s)	10
Spectral width (MHz)	1
Filter width (MHz)	2

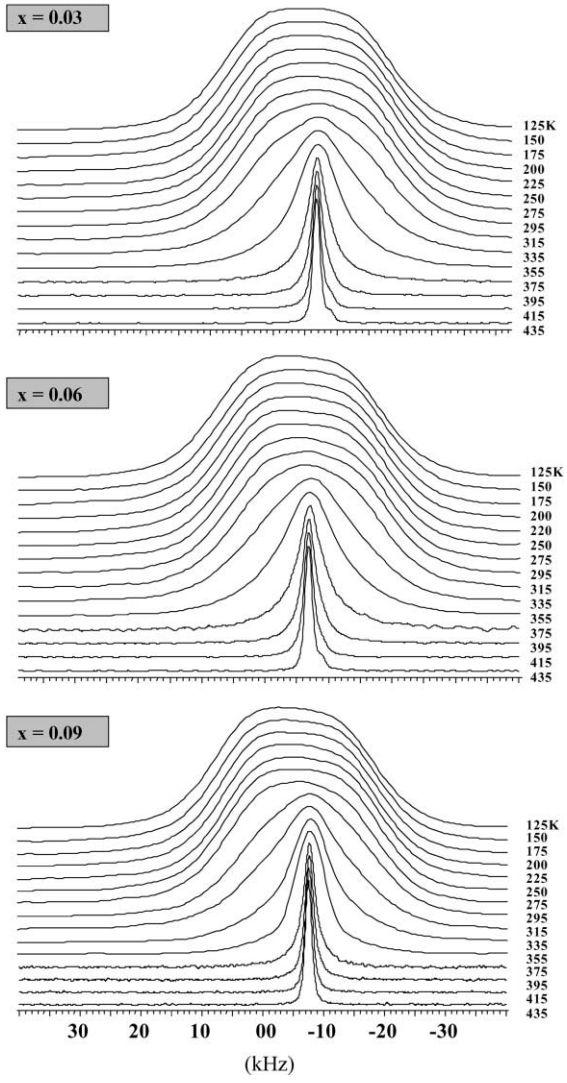

Fig. 1. Thermal variation of the ^{19}F NMR spectrum (kHz) between 125 and 435 K for the $Pb_{1-x}Mg_xF_2$ compositions relative to $x = 0.03$, 0.06 and 0.09.

3. ^{19}F NMR results

The ^{19}F NMR spectra at various temperatures between 125 and 435 K are given for $x = 0.03, 0.06$ and 0.09 in Fig. 1: at very low temperatures, the ^{19}F NMR spectra appear, whatever x, as the envelop of two peaks, labeled p_1 and p_3, localized, respectively, at $\approx 3 \pm 1$ and $\approx 14 \pm 2$ kHz. The origin of the frequency scale corresponds to the nominal iradiation frequency (188.283 MHz). Above $T \approx 275$ K, a third peak, called p_2, located between the p_1 and p_3 peaks can be observed; p_2 is growing with rising temperature at the detriment of p_1 and p_2 peaks. Beyond $T \approx 375$ K, the p_2 peak is discernable only.

The relative contributions of the different peaks observed at each temperature are determined by deconvolution of the whole spectrum. Whatever x, the lower temperature spectrum at $T = 125$ K, has been deconvoluted, in a first time, on the basis of Gaussian functions for the p_1 and p_3 peaks; but, whatever the adjustment parameters, a non-negligible residue results from the deconvolution. An accurate simulation has been obtained, in a second time, taking into account a supplementary contribution of a Lorentzian type function representative of the p_2 peak, as for the higher temperature spectra relative to ($275 \leq T \leq 375$ K) range. Finally, whatever $T \leq 375$ K, the ^{19}F NMR spectrum consists of three contributions, these of p_1 and p_3, which represent fluoride ions, fixed on the NMR time scale and that of p_2 which corresponds to mobile fluoride ions. Above $T \approx 375$ K, all F^- ions are mobile on the NMR time scale. Fig. 2 gives, for example, the deconvolution of the ^{19}F NMR spectrum of $Pb_{1.97}Mg_{0.03}F_2$ at 125 and 335 K. The results of deconvolution of the ^{19}F NMR spectra and the percentages of F^- ions

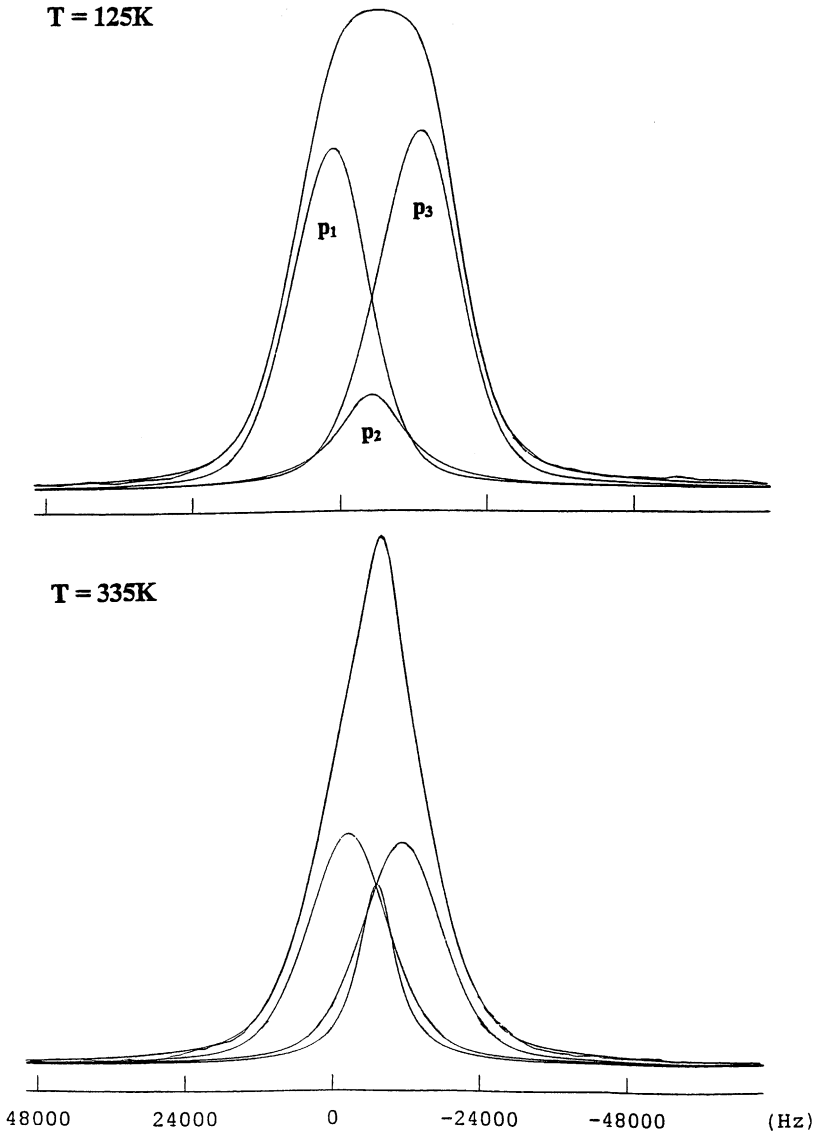

Fig. 2. Deconvolution of the ^{19}F NMR spectrum of $Pb_{0.97}Mg_{0.03}F_2$ at 125 and 335 K: (—) deconvoluted spectrum.

Table 2
Results of deconvolution of the ^{19}F NMR spectrum of $Pb_{1-x}Mg_xF_2$ compositions at different temperatures between 125 and 435 K

$Pb_{0.97}Mg_{0.03}F_2$							$Pb_{0.94}Mg_{0.06}F_2$							$Pb_{0.91}Mg_{0.09}F_2$						
T (K)	Position (±0.2 kHz)			$\Delta\nu/2$ (±0.2 kHz)			T (K)	Position (±0.2 kHz)			$\Delta\nu/2$ (±0.2 kHz)			T (K)	Position (±0.2 kHz)			$\Delta\nu/2$ (±0.2 kHz)		
	p_1	p_2	p_3	p_1	p_2	p_3		p_1	p_2	p_3	p_1	p_2	p_3		p_1	p_2	p_3	p_1	p_2	p_3
125	2.6	−4.5	−15.8	14.7	13.2	15.8	125	1.9	−5.3	−15.9	15.0	14.7	15.0	125	1.2	−6.4	−15.5	14.8	15.3	14.3
150	1.9	−4.9	−15.7	14.7	12.8	15.8	150	0.8	−5.8	−15.5	14.7	15.0	14.7	150	1.0	−7.5	−15.6	14.7	15.0	13.9
175	0.8	−6.6	−15.8	14.8	13.5	15.6	175	0.4	−6.0	−15.7	15.0	15.0	14.7	175	0.8	−7.9	−15.8	15.0	15.0	13.9
200	0.3	−6.8	−15.4	14.7	13.5	15.6	200	00	−7.5	−15.4	15.0	14.7	14.8	200	0.5	−8.3	−15.8	15.0	14.3	13.8
225	0.0	−6.9	−15.5	14.8	12.8	15.8	225	00	−8.3	−15.4	15.0	14.8	14.5	225	0.1	−8.5	−15.6	14.8	14.3	14.3
250	−0.3	−7.2	−15.3	15.0	13.2	15.6	250	−0.8	−8.7	−15.8	15.0	13.9	14.9	250	0.2	−8.5	−15.0	15.0	14.5	13.8
275	−1.5	−7.5	−15.8	14.7	13.2	15.7	275	−0.8	−8.8	−15.6	15.0	13.5	14.5	275	00	−8.2	−14.8	15.0	14.3	13.5
295	−1.8	−7.9	−15.0	15.0	11.3	15.4	295	−0.8	−8.2	−15.2	15.0	13.0	14.5	295	−0.8	−7.5	−15.0	14.8	12.0	13.2
315	−2.0	−8.0	−15.0	15.0	10.5	15.3	315	−1.2	−7.5	−14.7	15.0	12.0	14.3	315	−1.5	−7.3	−15.4	14.3	10.5	12.5
335	−2.3	−7.5	−12.4	15.0	8.3	15.0	335	−1.5	−7.2	−13.9	14.3	11.3	12.8	335	−1.9	−7.2	−15.4	12.0	7.5	12.0
355	−2.3	−7.0	−12.0	12.0	7.9	13.5	355	−1.6	−6.8	−13.5	10.5	9.0	10.5	355	−2.0	−7.0	−15.0	10.2	6.0	10.1
375	−2.3	−6.8	−12.0	8.0	4.2	10.0	375	−1.8	−6.8	−13.0	7.5	4.2	7.5	375	–	−7.0	–	–	2.5	–
395	–	−6.8	–	–	2.4	–	395	–	−6.8	–	–	3.0	–	395	–	−7.0	–	–	1.8	–
415	–	−6.8	–	–	1.7	–	415	–	−6.8	–	–	1.9	–	415	–	−7.0	–	–	1.5	–
435	–	−6.8	–	–	1.5	–	435	–	−6.8	–	–	1.5	–	435	–	−7.0	–	–	1.5	–

proportional to areas of different peaks are given for each temperature studied in Tables 2 and 3, respectively.

Temperature dependence of ($\Delta\nu/2$), linewidth of the ^{19}F NMR spectrum, is given for $Pb_{0.94}Mg_{0.06}F_2$, for instance, in Fig. 3. The experimental points are located on a curve, which can be simulated by a Boltzmann function [22]

$$\Delta\nu/2(T) = \Delta\nu_r + \frac{\Delta\nu_R - \Delta\nu_r}{1 + \exp[(T - T_0)/\Delta T]} \quad (1)$$

where $\Delta\nu_r$ is a residual half-width due to the field inhomogeneity at T_{max} (≈435 K); $\Delta\nu_R$ the half-width of the rigid lattice; T_0 the center of the Boltzman function and $--\Delta T = \sum(T_j - T_i)/n$ is the average temperature difference between two successive experimental temperatures T_i and T_j, with $(n + 1)$ the number of measurement temperatures.

The calculated parameters for the simulation function are reported for three compositions ($x = 0.03$, 0.06, 0.09) in Table 4. The value of each parameter can be considered as independent of x.

Above $T \approx 275$ K, $\Delta\nu/2$ decreases progressively at rising temperature. This narrowing is due to mobile F^- ion motions that average out the F–F dipolar interactions. The activation energy of F^- ions mobile on the NMR time scale has been calculated from the thermal variation of the jump frequency ν_s. Linenarrowing occurs when the F^- ion jump frequency ν_s is of the same order as the rigid lattice linewidth. The thermal variation of ν_s can be deduced from that of $\Delta\nu/2$

Table 3
Areas (%) of different peaks (p_i) and numbers of fluoride ions (nF_i) corresponding to these percentages at different temperatures

$Pb_{0.97}Mg_{0.03}F_2$							$Pb_{0.94}Mg_{0.06}F_2$							$Pb_{0.91}Mg_{0.09}F_2$						
T (K)	p_1% (±3)	p_2% (±3)	p_3% (±3)	nF_1	nF_2	nF_3	T (K)	p_1% (±3)	p_2% (±3)	p_3% (±3)	nF_1	nF_2	nF_3	T (K)	p_1% (±3)	p_2% (±3)	p_3% (±3)	nF_1	nF_2	nF_3
125	48	14	38	0.96	0.28	0.76	125	43	20	37	0.86	0.40	0.74	125	35	35	30	0.70	0.70	0.60
150	49	13	38	0.98	0.26	0.76	150	42	21	37	0.84	0.42	0.74	150	34	34	32	0.68	0.68	0.64
175	49	15	36	0.98	0.30	0.72	175	42	21	37	0.84	0.42	0.74	175	35	34	31	0.70	0.68	0.62
200	49	14	37	0.98	0.28	0.74	200	43	22	35	0.86	0.44	0.70	200	35	35	30	0.70	0.70	0.60
225	49	14	37	0.98	0.28	0.74	225	44	23	33	0.88	0.46	0.66	225	36	33	31	0.72	0.66	0.62
250	48	14	38	0.96	0.28	0.76	250	44	22	34	0.88	0.44	0.68	250	35	34	31	0.70	0.68	0.62
275	49	13	38	0.98	0.26	0.76	275	44	23	33	0.88	0.46	0.66	275	34	35	31	0.68	0.70	0.62
295	48	13	39	0.96	0.26	0.78	295	44	22	34	0.88	0.44	0.68	295	31	37	32	0.62	0.74	0.64
315	45	19	36	0.90	0.38	0.72	315	41	27	32	0.82	0.54	0.64	315	27	56	17	0.54	1.12	0.34
335	41	26	33	0.82	0.52	0.66	335	31	46	23	0.62	0.92	0.46	335	11	78	11	0.22	1.56	0.22
355	11	78	11	0.22	1.56	0.22	355	10	80	10	0.20	1.60	0.20	355	2	96	2	0.04	1.92	0.04
375	2	96	2	0.04	1.92	0.04	375	3	93	4	0.06	1.86	0.08	375	0	100	0	0	2	0
395	0	100	0	0	2	0	395	0	100	0	0	2	0	395	0	100	0	0	2	0
415	0	100	0	0	2	0	415	0	100	0	0	2	0	415	0	100	0	0	2	0
435	0	100	0	0	2	0	435	0	100	0	0	2	0	435	0	100	0	0	2	0

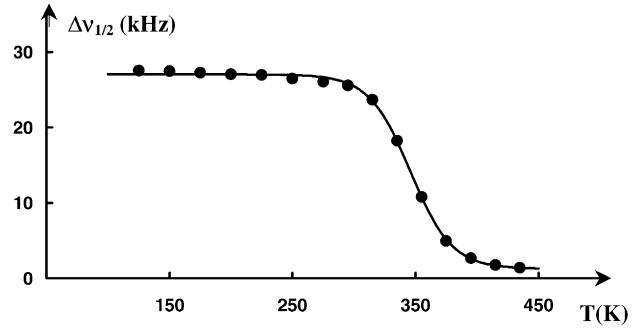

Fig. 3. Temperature dependence of $\Delta\nu/2$ (kHz) for $Pb_{0.94}Mg_{0.06}F_2$.

Table 4
Simulation function parameters of $\Delta\nu/2$ for the different $Pb_{1-x}Mg_xF_2$ compositions

	$x = 0.03$	$x = 0.06$	$x = 0.09$
$\Delta\nu_R$ (kHz)	27.1 ± 0.1	27.0 ± 0.2	27.3 ± 0.2
$\Delta\nu_r$ (kHz)	1.3 ± 0.2	1.3 ± 0.2	1.3 ± 0.3
T_0 (K)	340 ± 2	346 ± 2	320 ± 2
ΔT (K)	16 ± 1	17 ± 1	19 ± 1

by the expression [23]

$$\nu_s = \frac{\alpha|\Delta\nu/2 - \Delta\nu_r|}{\tan[(\pi/2)|(\Delta\nu/2 - \Delta\nu_r)/(\Delta\nu_R - \Delta\nu_r)|^2]} \quad (2)$$

where the different parameters $\Delta\nu/2$, $\Delta\nu_r$, $\Delta\nu_R$ are the same as in the Eq. (1) and the term α ($\approx$1) is a constant function of the line shape.

The inverse temperature dependence of ν_s over the range ($150 < T < 355$ K) is given for $Pb_{0.91}Mg_{0.09}F_2$, for instance, in Fig. 4. A linear fit to $\nu_s = \nu_0 \exp(-\Delta E_{NMR}/kT)$ is shown, with correlation coefficient equal to 0.98, first between 150 and 250 K, then between 250 and 355 K. In these both temperature ranges, ν_s exhibits an Arrhenius-type behavior. The activation energies, ΔE_{NMR}, equal to 0.06 and 0.27 eV in the low- and high-temperature ranges, respectively, are clearly less than that of ΔE_σ determined by impedance spectroscopy and equal to $\approx$0.37 eV in the ($280 < T < 380$ K) temperature range [18]. As ΔE_σ is determined from the temperature dependence of σ_{dc}, the motions corresponding to ΔE_σ are long range; equally in return, considering the very high value of the frequency of NMR spectrometer (Table 1), the F^- ion motions on the NMR time scale are short range. The ΔE_{NMR} values determined for three compositions studied are gathered in Table 5: they do not vary significantly with x and characterize consequently local motions of same type in three compositions studied.

Table 5
Comparison of activation energies determined by ^{19}F NMR and impedance spectroscopy for the different $Pb_{1-x}Mg_xF_2$ compositions

x	Temperature range (K)	ΔE_{NMR}[a]	ΔE_σ [13,14]
0.03	150–250	0.06 ± 0.01	–
	250–360	0.28 ± 0.02	–
	280–380	–	0.37 ± 0.02
0.06	150–250	0.06 ± 0.01	–
	250–360	0.27 ± 0.02	–
	280–380	–	0.37 ± 0.02
0.09	150–250	0.06 ± 0.01	–
	250–360	0.26 ± 0.02	–
	280–380	–	0.37 ± 0.02

[a] This work.

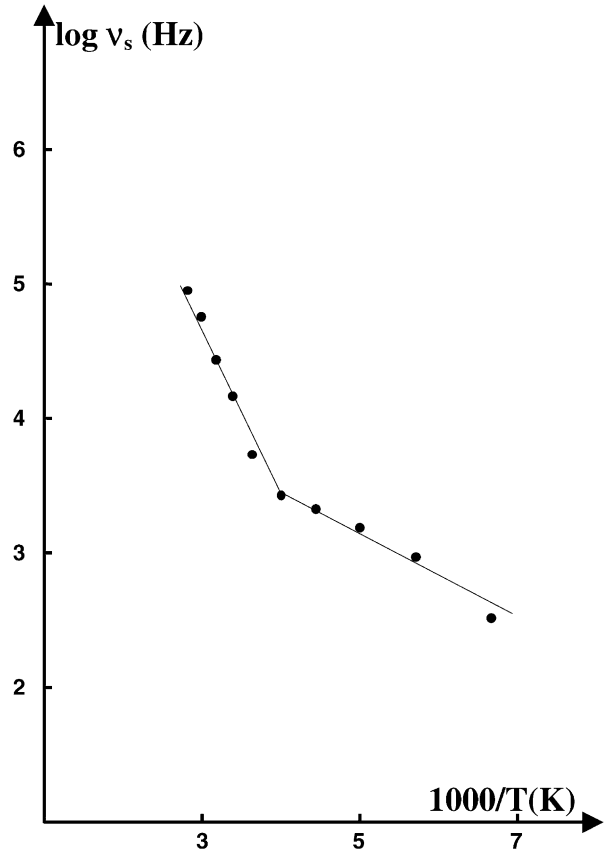

Fig. 4. Inverse temperature dependence of log ν_s (Hz) for $Pb_{0.91}Mg_{0.09}F_2$.

4. Discussion

The deconvolution of the ^{19}F NMR spectrum relative to $T = 125$ K has shown the presence of three fluoride sublattices in each $Pb_{1-x}Mg_xF_2$ sample studied: the one, corresponding to p_2, is mobile at that temperature; both others, represented by p_1 and p_3 are fixed. The numbers of F^- ions per formula unit, $nF_1(T)$, $nF_2(T)$ and $nF_3(T)$, proportional to p_1, p_2 and p_3% can be calculated from following equations:

$$\frac{nF_1(T)}{p_1\%} = \frac{nF_2(T)}{p_2\%} = \frac{nF_3(T)}{p_3\%} = \frac{2}{1000} \quad (3)$$

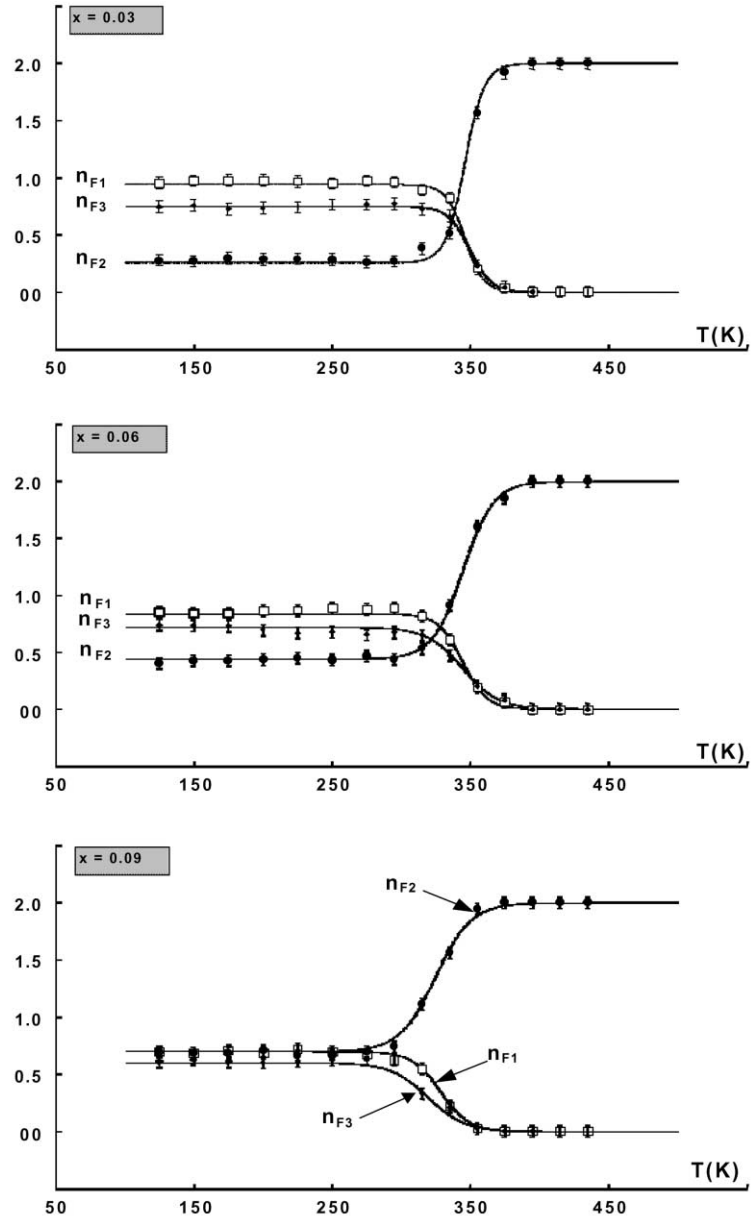

Fig. 5. Temperature dependence of $nF_1(T)$, $nF_2(T)$, $nF_3(T)$ for the $Pb_{1-x}Mg_xF_2$ compositions relative to $x = 0.03$, 0.06 and 0.09.

Temperature dependences of $nF_1(T)$, $nF_2(T)$, $nF_3(T)$ are given, for each composition, in Fig. 5. The points representative of $nF_1(T)$ and $nF_3(T)$ are located on a curve, which can be simulated, as $\Delta v/2$, by a Boltzmann function

$$nF_j(T) = n(F_j)_r + \frac{n(F_j)_R - n(F_j)_r}{1 + \exp[(T - T_0)/\Delta T]} \quad (F_j = F_1, F_3) \tag{4}$$

The curve relative to $nF_2(T)$ is, on the contrary, simulated by an inverse Boltzmann function of type

$$nF_2(T) = n(F_2)_r - \frac{n(F_2)_r - n(F_2)_R}{1 + \exp[(T - T_0)/\Delta T]} \tag{5}$$

The calculated parameters for the simulation functions are reported for three compositions in Table 6. Considering the low temperature range (125–275 K) in Fig. 5, it is interesting to note that, whatever x, the number of F^- ions in each sublattice is quasi-constant and equal to $n(F)_R$ in a wide temperature range. Independently of diffusion properties, three sublattices can be considered as distinct on a structural point of view.

Composition dependence of $n(F)_R$, is given in Fig. 6 for each sublattice. The increase of $n(F_2)_R$ with x is linear and is of ($y = 8x$) type; on the contrary, $n(F_1)_R$ and $n(F_3)_R$ decrease when x increases. Supposing that the fluoride ions located in the normal positions of the fluorite are the F_1 anions, $n(F_1)_R$, equal to 2 for $x = 0$, decreases quickly for $0 < x < 0.03$

Table 6
Simulation function parameters of $nF_1(T)$, $nF_2(T)$, $nF_3(T)$ for the different $Pb_{1-x}Mg_xF_2$ compositions

	$x = 0.03$	$x = 0.06$	$x = 0.09$
$n(F_1)_R$	0.98 ± 0.02	0.84 ± 0.02	0.70 ± 0.02
$n(F_1)_r$	0.01 ± 0.01	0.01 ± 0.01	0.01 ± 0.01
T_0 (K)	346 ± 2	344 ± 2	328 ± 2
ΔT (K)	7 ± 1	10 ± 1	10 ± 1
$n(F_2)_R$	0.26 ± 0.02	0.44 ± 0.02	0.70 + 0.02
$n(F_2)_r$	2.00 ± 0.02	2.00 ± 0.02	2.00 ± 0.02
T_0 (K)	346 ± 2	344 ± 2	324 ± 2
ΔT (K)	7 ± 1	11 ± 1	13 ± 1
$n(F_3)_R$	0.76 ± 0.02	0.72 ± 0.02	0.60 ± 0.02
$n(F_3)_r$	0.01 ± 0.01	0.01 ± 0.01	0.01 ± 0.01
T_0 (K)	349 ± 2	344 ± 2	319 ± 2
ΔT (K)	8 ± 1	13 ± 1	13 ± 1

(dotted line), then more slowly for $0.03 < x < 0.09$. It results from the composition dependences of $n(F_1)_R$ and $n(F_2)_R$ that $n(F_3)_R$, equal to 0 for $x = 0$, increases first quickly with x, is maximum for a value of $x \leq 0.03$ (dotted line), then decreases for $0.03 < x < 0.09$.

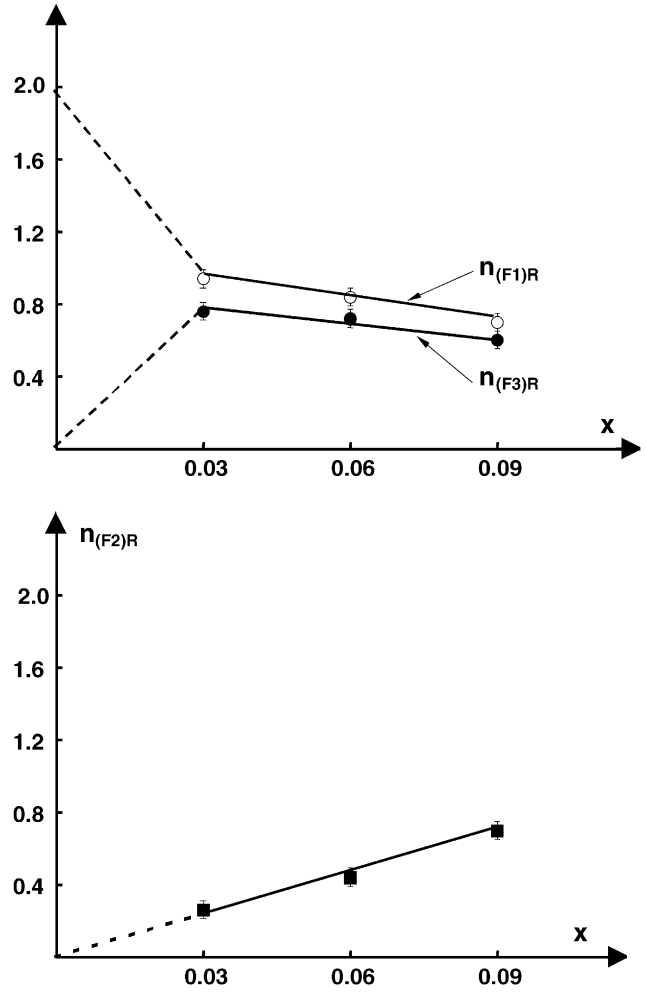

Fig. 6. Composition dependence of $n(F_1)_R$, $n(F_2)_R$, $n(F_3)_R$.

In order to precise the nature of three sublattices, we have examined the extended defects in $Pb_{1-x}Mg_xF_2$ from following considerations.

- It is well known that the Mg^{2+} cations generally offer a coordination number (CN) equal to 6 in most magnesium binary or ternary fluorides [24].
- For a PbF_2-β lattice Pb has cubic coordination PbF_8, the change of a (CN 8) of the Pb^{2+} ion to (CN 6) for the Mg^{2+} ion involves the transfer of two fluorine atoms from normal into interstitial sites.

Fig. 7 gives the (xOy) projection of the fluorite unit cell, where one Pb^{2+} ion is replaced by one Mg^{2+} ion of smaller size. Though a_c does not vary notably with x, that substitution results in important local distortions due to the large size difference between both cations: $r(Pb^{2+})$ in (CN 8) = 1.43 Å, $r(Mg^{2+})$ in (CN 6) = 0.86 Å [25]. A calculation of the Mg–F_n and F_n–F_n distances indicates that the values obtained, $d_{Mg-F_n} \approx 2.56-2.57$ Å and $d_{F_n-F_n} \approx 2.96-2.97$ Å, are respectively, clearly higher than d_{Mg-F} (≈1.98–2.00 Å) and d_{F-F} (≈2.38 Å) in MgF_2 of rutile structure [26]. Shorter d_{Mg-F_n} and $d_{F_n-F_n}$ distances can be calculated by supposing a relaxation of six F_n^- fluoride ions from their starting position (1/4, 1/4, 1/4) towards the Mg^{2+} central cation (0, 0, 0) (Fig. 7). Both other F_n^- fluoride ions, shifting in interstitial sites, draw nearer to Pb^{2+} ions resulting, close to cluster, in coordination (6 + 2) and (8 + 1) for the Mg^{2+} and Pb^{2+} ions, respectively. The substitution model which derives from these considerations:

$$Pb^{2+} + 8F_n^- \rightarrow Mg^{2+} + 6F_r^- + 2F_i^- + 8\bullet \quad (\bullet = \text{vacancy})$$

is in agreement with the variation of $n(F_2)_R$ with x. As a matter of fact, the F_r^- and F_i^- ions, different from the structural point of view, are not distinguished by ^{19}F NMR investigation, because both fluoride ion types are yet mobile at very low temperature ($T = 125$ K).

The formation of this elementary cluster around the Mg^{2+} ion, labeled "$MgPb_7$", results also in local deformations, less important but not negligible, in a second zone (dark zone in Fig. 7), where there are Pb^{2+} and F^- ions located at $d \approx a_c$ from the central Mg^{2+} ion. The number of F^- ions in that zone, which could be considered as the F_3 sublattice, is equal to 24, the other F^- ions, farther from defect, forming the F_1 normal sublattice. The presence of the "$MgPb_7$" cluster results in following calculated values for $x = 0.03$:

$$x = 0.03: n(F_1) = 1.04, \qquad n(F_2) = 0.24, \qquad n(F_3) = 0.72$$

Comparison of the calculated values to these of $n(F_1)_R$, $n(F_2)_R$ and $n(F_3)_R$, respectively (in Table 6), shows the validity of this cluster for that x value. But, for higher x values, the results obtained for $n(F_3)$ and consequently for $n(F_1)$ are not in agreement and a more extended cluster must be then investigated.

The association of such monomer clusters inside column clusters cannot be selected in $Pb_{1-x}Mg_xF_2$, because $n(F_2)_R$ would not verify then the ($y = 8x$) equation. Consequently,

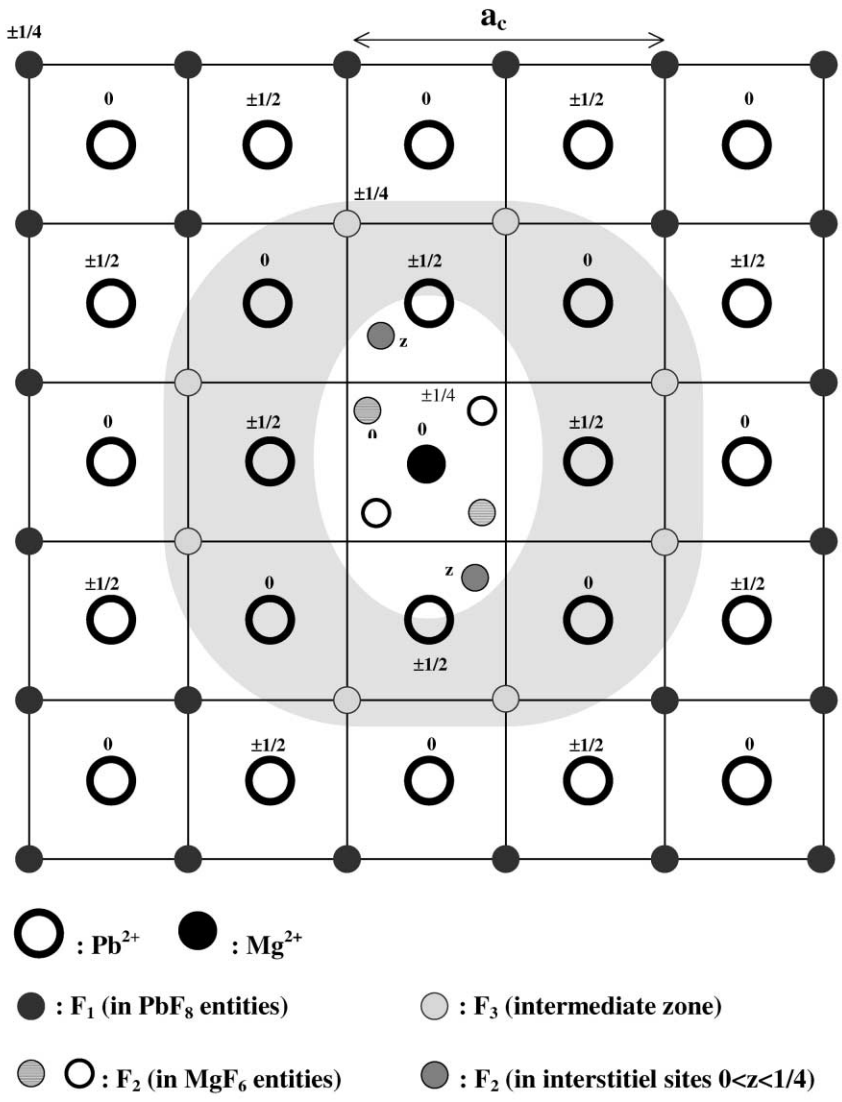

Fig. 7. Projection on xOy of the "$MgPb_7$" cluster proposed for $x = 0.03$.

we are interested in isolated more extended clusters and involving a smaller content of F^- ions inside the F_3 sublattice. An unit cell of fluorite type has been investigated in which the Pb atoms located in height corners are replaced by Mg atoms (Fig. 8). This extended cluster is labeled "$MgPb_3$". The values of $n(F_j)$ calculated for $x = 0.06$ from that hypothesis are the following:

$$x = 0.06: n(F_1) = 0.80, \qquad n(F_2) = 0.48, \qquad n(F_3) = 0.72$$

These results are in good agreement with the values of $n(F_1)_R$, $n(F_2)_R$, $n(F_3)_R$ in Table 6, proving the validity of this extended cluster for $x = 0.06$.

The value of $n(F_3)_R$ obtained for $x = 0.09$ is relatively weaker than that corresponding to $x = 0.06$. One can suppose that the number of extended clusters proposed for $x = 0.06$ is important enough in order that interactions between them take place resulting in the formation of bigger clusters and the decrease of F^- ion content in the intermediate zone.

That proposition of "$MgPb_7$" clusters for low x values ($x = 0.03$) and "$MgPb_3$" clusters for higher x values ($x = 0.06$) has allowed to identify three sublattices of F^- ions, which have been detected in $Pb_{1-x}Mg_xF_2$ by ^{19}F NMR.

The (F_2) sublattice, very distorted, completely implicated by the substitution of the Mg^{2+} ion to Pb^{2+} one, the (F_3) intermediate sublattice, disturbed to a lower degree and the (F_1) sublattice which is not influenced by the substitution mode.

Temperature dependence of the jump frequency, v_s, has shown the existence of two F^- ion distinct motions on the NMR time scale characterized by activation energies ΔE_{NMR} equal to 0.06 eV in the 150–250 K range and 0.27 eV in the 250–360 K range. It is probable that, in the lower temperature range, it concerns F^- ion exchange motions inside (F_2) sublattice and in the higher temperature range, exchange motions between (F_3) and (F_2) sublattices [27].

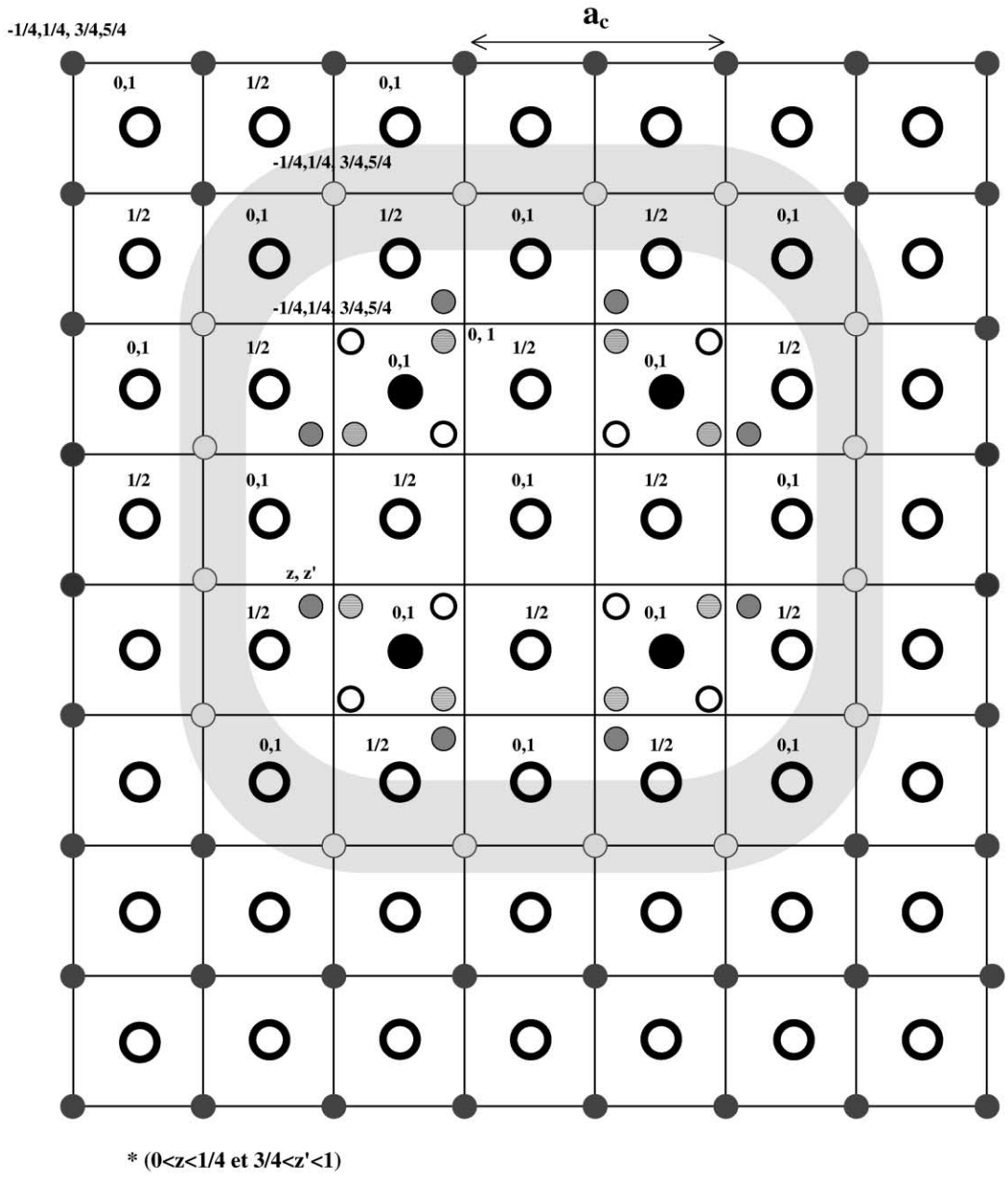

Fig. 8. Projection on xOy of the "$MgPb_3$" cluster proposed for $x = 0.06$.

5. Conclusions

The ^{19}F NMR investigation of different compositions of the $Pb_{1-x}Mg_xF_2$ solid solution has allowed to prove the existence of three distinct fluoride sublattices. The variation of numbers of fluoride ions belonging to each fluoride sublattice has been determined as a function of temperature for three compositions relative to $x = 0.03$, 0.06 and 0.09. Clusters have been proposed from the composition dependence of the anionic distribution determined by deconvolution of the low temperature ^{19}F NMR spectra.

The first sublattice, labeled (F_2), very distorted, includes the relaxed (F_r^-) and interstitial (F_i^-) anions located in the surroundings of Mg^{2+} cations. These anions different from the structural point of view are mobile at very low temperatures and consequently cannot be distinguished by ^{19}F NMR investigation. The variation of $n(F_2)$ with x is of ($y = 8x$) type, in agreement with the substitution model

$$Pb^{2+} + 8F_n^- \rightarrow Mg^{2+} + 6F_r^- + 2F_i^- + 8\bullet \quad (\bullet = \text{vacancy})$$

The other fluoride sublattices, labeled (F_1) and (F_3), represent respectively the sublattice of F^- ions in normal positions of the fluorite which is not influenced by the substitution mode and an intermediate sublattice located between the (F_2) and (F_1) sublattices and disturbed to a lower degree than (F_2) by the substitution of Mg^{2+} ion to Pb^{2+} ion.

The activation energies ΔE_{NMR} deduced from the temperature dependence of the F^- ion jump frequency, equal to 0.06 eV in the 150–250 K range and 0.27 eV in the 250–360 K range are clearly less than ΔE_σ determined by impedance spectroscopy and it results that the F^- ion motions on the NMR time scale are short range. It concerns F^- ion exchange motions inside (F_2) sublattice in the lower temperature range, then exchange motions between (F_2) and (F_3) sublattices in the higher temperature range.

References

[1] J.M. Réau, J. Sénégas, M. El Omari, J. Solid State Chem. 84 (1990) 253.
[2] J.M. Réau, M. Wahbi, J. Sénégas, P. Hagenmuller, Physica Status Solidi B 169 (1992) 331.
[3] J.M. Réau, P. Hagenmuller, Rev. Inorg. Chem. 19 (1999) 45.
[4] C.R.A. Catlow, J. Phys. C 9 (1976) 1845.
[5] J. Corish, C.R.A. Catlow, P.W.M. Jacobs, S.H. Ong, Phys. Rev. B 25 (1982) 6425.
[6] J.P. Laval, A. Mikou, B. Frit, G. Roult, Solid State Ionics 28–30 (1988) 1300.
[7] A.K. Cheetham, B.E.F. Fender, B. Steele, R.I. Taylor, B.T.M. Willis, Solid State Commun. 8 (1970) 171.
[8] M. El Omari, J.L. Soubeyroux, J. Sénégas, J.M. Réau, Solid State Ionics 130 (2000) 133.
[9] J.L. Soubeyroux, J.M. Réau, M. Wahbi, J. Sénégas, S.K. Soo, Solid State Commun. 82 (1992) 63.
[10] M. El Omari, J.M. Réau, J. Sénégas, J. Solid State Chem. 87 (1990) 430.
[11] J.M. Réau, X.Y. Jun, J. Sénégas, P. Hagenmuller, Solid State Ionics 78 (1995) 315.
[12] C. Lucat, A. Rhandour, L. Cot, J.M. Réau, Solid State Commun. 32 (1979) 167.
[13] M. El Omari, J. Sénégas, J.M. Réau, Solid State Ionics 100 (1997) 233.
[14] M. El Omari, J. Sénégas, J.M. Réau, Solid State Ionics 100 (1997) 241.
[15] F. Wang, C.P. Grey, J. Am. Chem. Soc. 117 (1995) 6637.
[16] F. Wang, C.P. Grey, Chem. Mater. 9 (1997) 1068.
[17] F. Wang, C.P. Grey, J. Am. Chem. Soc. 120 (1998) 970.
[18] V. Trcovcova, P.P. Fedorov, I.I. Buchinskaya, V. Smatko, F. Hanic, Solid State Ionics 119 (1999) 181.
[19] ONEPULSE program, Bruker Spectrospin S.A., Wissembourg, France. Products for Spectrometer Type MSL-200.
[20] WINNMR 1D program, Bruker Spectrospin S.A., Wissembourg, France. 1D NMR data Processing, Version 950901.1, No. SPP-501.
[21] WINFIT program, Bruker Spectrospin S.A., Wissembourg, France. Line Shape Fitting, Version 9504 25, No. SPP-505.
[22] M. El Omari, J.M. Réau, J. Sénégas, J. Ravez, S.C. Abrahams, A. Nadiri, A. Yacoubi, J. Chem. Phys. 108 (1998) 2896.
[23] N. Blooembergen, E.M. Purcell, R.V. Pound, Phys. Rev. 73 (1948) 679.
[24] D. Babel, A. Tressaud, in: P. Hagenmuller (Ed.), Inorganic Solid Fluorides, Academic Press, New York, 1985, Chapter 3, p. 77.
[25] R.D. Shannon, Acta Crystallogr. A32 (1976) 751.
[26] W.H. Baur, Acta Crystallogr. B32 (1976) 2200.
[27] J. Sénégas, J.P. Laval, B. Frit, J. Fluorine Chem. 32 (1986) 197.